FRONTIERS OF PHYSICS

VIEW & PERSPECTIVE
Volume 22 / Issue 1 / 012401 / 2027

Engineering light–matter interactions with nanophotonic structures

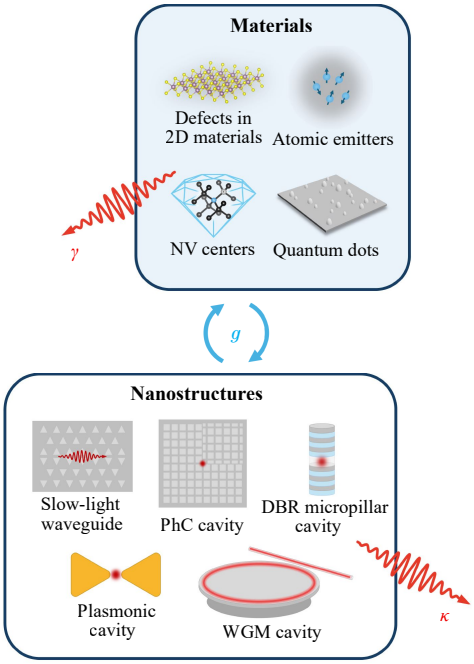
Kaifeng Zhang[1], Hancong Li[1], Xiulai Xu[1,2,†]

1 State Key Laboratory for Mesoscopic Physics and Frontiers Science Center for Nano-optoelectronics, School of Physics, Peking University, Beijing 100871, China
2 Collaborative Innovation Center of Extreme Optics, Shanxi University, Taiyuan 030006, China
Corresponding author. E-mail: †xlxu@pku.edu.cn
Received October 10, 2026; accepted October 20, 2026

© Higher Education Press 2027

ABSTRACT

Engineering light–matter interactions at the nanoscale is a central goal of modern photonics, underpinning advances in quantum technologies, nonlinear optics, sensing, and integrated optoelectronics. Nanophotonic structures provide a powerful route to reshape the electromagnetic environment, enabling control over spontaneous emission, optical confinement, photon extraction, and coherent photon–matter dynamics across weak- and strong-coupling regimes. Here, we review representative quantum-emitter platforms and nanophotonic architectures, comparing their respective strengths and limitations in terms of application suitability and practical considerations, such as integration potential and fabrication complexity. For devices combining quantum emitters with nanophotonic structures, particular emphasis is placed on the gap between ideal optical metrics and experimentally measured performance, arising from spatial, spectral, and polarization mismatch, dissipation, fabrication imperfections, and material constraints. These considerations connect fundamental light–matter interactions to applications ranging from quantum light sources and optical sensing to cavity quantum electrodynamics interfaces and quantum simulation. Future progress will increasingly rely on the co-design of quantum emitters, electromagnetic modes, and output channels, rather than the isolated optimization of individual photonic structures.



Keywords light-matter interaction, nanophotonic structure

Light–matter interaction lies at the foundation of spectroscopy, photochemistry, optoelectronics, nonlinear optics, and quantum information science [1]. For an isolated emitter interacting with a selected free-space optical mode, however, the interaction is typically weak because a diffraction-limited field extends over a spatial scale much larger than the emitter, and only a small fraction of the incident optical mode couples efficiently to its dipolar transition [2]. Engineering the electromagnetic environment therefore provides a powerful route to control the strength of light–matter interaction, thereby modifying the optical transition rates or coherent photon–matter dynamics.

The behavior of the light and matter depends on the relation between coherent coupling and dissipation, giving rise to distinct interaction regimes. In the weak-coupling regime, a central example of this environmental control is the Purcell effect [3], where the coherent emitter–cavity coupling rate g is small compared with the dissipative rates, including the cavity decay rate κ and the emitter decoherence rate γ. The cavity primarily modifies irreversible spontaneous emission processes through the local density of optical states (LDOS). For a narrowband emitter resonant with a single cavity mode, located at the field maximum and aligned with the local polarization, the enhancement can be assessed through the ideal

https://doi.org/10.15302/frontphys.2027.012401

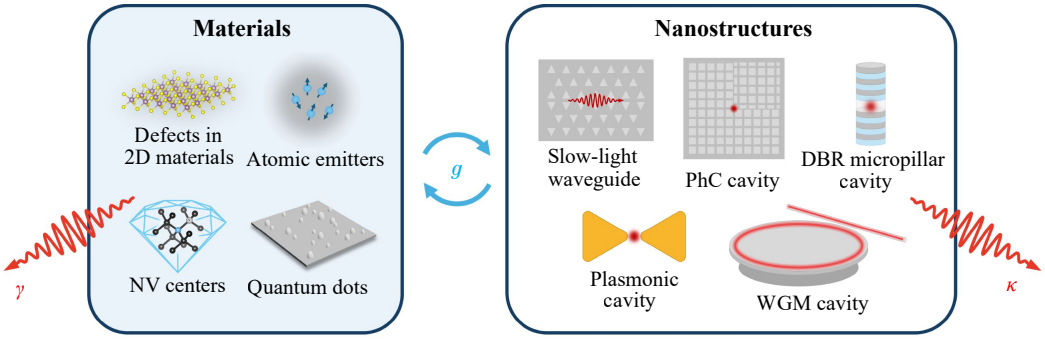


Fig. 1 Representative quantum-emitter platforms and nanophotonic structures for enhanced light–matter interactions, with a schematic illustration of coupling and dissipation.

Purcell factor:

$$F_{\mathrm{P}}^{\mathrm{ideal}} = \frac{3}{4\pi^2}\left(\frac{\lambda}{n}\right)^3 \frac{Q}{V}. \tag{1}$$

Here, Q is the cavity quality factor and V is the effective optical mode volume. A high Q increases the photon storage time and sharpens the optical resonance, whereas a small V increases the vacuum-field amplitude at the emitter. Purcell-enhanced emission can increase source brightness [4] and the fraction of emission directed into a desired optical mode, which may in turn contribute to improved single-photon purity and indistinguishability [5]. These advantages are particularly important for quantum light sources, including deterministic single-photon emitters. When coherent photon–matter exchange becomes comparable to or faster than the relevant loss and decoherence processes, the system enters the strong-coupling regime, in which optical and material excitations form hybrid eigenstates and give rise to phenomena such as vacuum Rabi oscillations and normal-mode splitting [6]. This ability to engineer light–matter interactions across different coupling regimes enables control over both irreversible emission and coherent dynamics, providing a versatile platform for fundamental studies [7] and applications in quantum photonics, nonlinear optics, sensing, and quantum information science [8].

For a quantum emitter system, the material platform determines the intrinsic properties including the optical transition strength, radiative efficiency, photon purity, coherence, and environmental sensitivity. These intrinsic characteristics, however, represent only one side of the light–matter interface. The surrounding photonic structure reshapes the electromagnetic environment and provides an additional degree of control over optical confinement, local density of states, emission directionality, and photon extraction efficiency [6]. The two complementary building blocks underlying engineered light–matter interactions, representative material platforms and photonic structures, are summarized in Fig. 1. Here we focus on semiconductor quantum dots (QDs), defects in two-dimensional (2D) materials, atomic systems, and solid-state color centers such as nitrogen–vacancy (NV) centers in diamond. On the photonic side, representative architectures include whispering-gallery-mode (WGM) cavities, photonic crystal (PhC) cavities, distributed-Bragg-reflector (DBR) micropillar cavities, plasmonic cavities, and slow-light PhC waveguides. Discussed material platforms and structures have all shown experimental demonstration, and their combination provides a broad design space in which the intrinsic properties of an emitter can be matched to the specific optical mode.

The optical properties of quantum emitters are critical to the performance of a given light–matter interface and ultimately determine its suitability for a particular application. The quantum emitter platforms are compared in terms of internal quantum efficiency η_{QE}, transition dipole moment μ, single-photon purity $g^{(2)}(0)$, photon indistinguishability $\mathcal{V}_{\mathrm{HOM}}$ and operating temperature T. The quantum efficiency η_{QE} represents the fraction of excited-state decays that occur through radiative rather than nonradiative processes. The transition dipole moment μ shows the intrinsic strength of the optical transition, which directly influences both the radiative transition rate and the emitter–field coupling strength. μ is usually inferred from observables such as radiative lifetime, oscillator strength and absorption strength [9, 10], or through theoretical calculation [11]. Single-photon purity characterizes the suppression of multi-photon emission events and is commonly quantified by the zero-delay second-order correlation $g^{(2)}(0)$ measured in a Hanbury Brown–Twiss experiment [6]. $g^{(2)}(0) = 0$ stands for an ideal single-photon source, and $g^{(2)}(0) < 0.5$ is commonly taken as evidence of antibunched single-emitter emission. Photon indistinguishability $\mathcal{V}_{\mathrm{HOM}}$ indicates whether photons from different photon emission events can interfere coherently. Finally, the operating temperature T reflects the thermal robustness of an emitter and strongly affects its practical accessibility.

As shown in Fig. 2(a), different quantum-emitter platforms exhibit distinct strengths and limitations, with no single platform outperforming the others across all

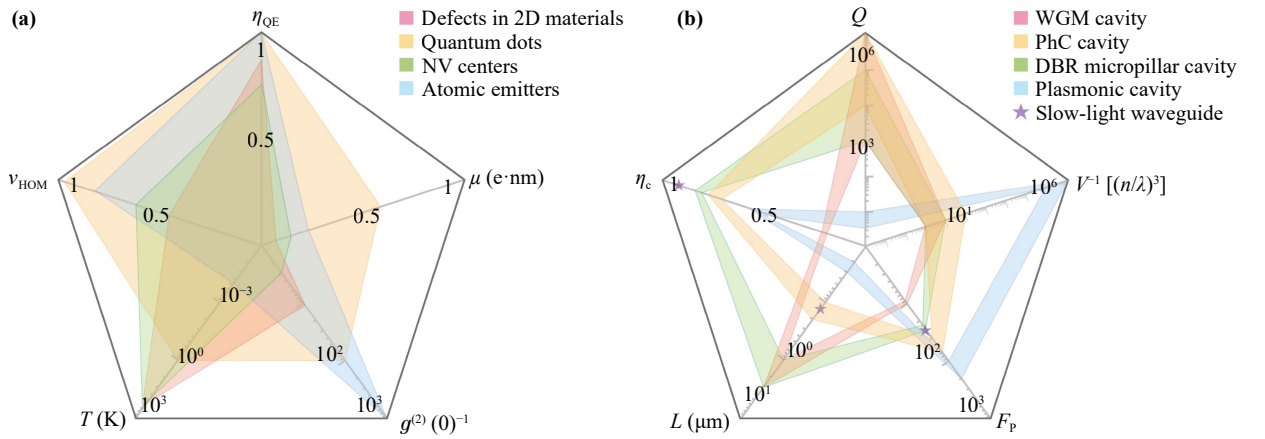


Fig. 2 Performance comparison of representative quantum-emitter platforms and nanophotonic structures. The relative importance of metrics considered here is application-dependent, and the comparison highlights the complementary strengths of different platforms rather than providing an overall performance ranking. **(a)** Material platforms are compared using five metrics. The internal quantum efficiency is $\eta_{QE} = \Gamma_r/(\Gamma_r + \Gamma_{nr})$, where Γ_r and Γ_{nr} are the radiative and nonradiative decay rates [12–14]. The transition dipole moment $\mu_{eg} = |\langle e|\hat{\boldsymbol{\mu}}|g\rangle|$ characterizes the strength of the optical transitions [9–11, 15]. Single-photon purity is quantified by the zero-delay second-order correlation $g^{(2)}(0)$ [14, 16–18]. Photon indistinguishability $\mathcal{V}_{HOM}$ is quantified by the Hong–Ou–Mandel interference visibility [6, 19–22]. The operating temperature T denotes the temperature range over which the relevant quantum emitter performance is retained. For the broad material classes shown here, the numerical ranges are based on representative and experimentally well-characterized systems rather than the entire material family. Demonstrated η_{QE}, $g^{(2)}(0)$ and $\mathcal{V}_{HOM}$ performances are selected from measurements without substantial Purcell enhancement, in order to reflect the intrinsic emitter performance as closely as possible. For the defects in 2D materials, the plotted values refer specifically to defect emitters in hBN. The presented metrics of NV centers mainly represent NV centers in bulk diamond, and the reported $\mathcal{V}_{HOM}$ for NV centers corresponds to two-photon interference between two separate NV centers [21]. **(b)** Photonic structures are compared using the quality factor $Q = \omega_0/\Delta\omega_0$ [6, 8, 23–26], effective mode volume $V = \int \epsilon(\boldsymbol{r})\,|\boldsymbol{E}(\boldsymbol{r})|^2\,\mathrm{d}^3\boldsymbol{r}/\max\left[\epsilon(\boldsymbol{r})\,|\boldsymbol{E}(\boldsymbol{r})|^2\right]$ [6, 8, 27], experimentally reported Purcell factor F_P [25, 28–31], structural collection efficiency $\eta_c = \beta\eta_{ex}$ [5, 23, 25, 30, 32–35], and critical feature size L. Here ω_0 stands for the central frequency of the cavity mode while $\Delta\omega_0$ represents its spectral linewidth, $\epsilon(\boldsymbol{r})$ and $\boldsymbol{E}(\boldsymbol{r})$ represent the local dielectric permittivity and electric field respectively, β is the coupling ratio into the selected optical mode and η_{ex} is the probability that it further exits through the selected output channel [12]. The displayed shaded range bands should be interpreted as representative experimental value ranges or characteristic scales rather than universal material or device constants. For plasmonic cavities, the conventional mode-volume definition used for dielectric cavities is not strictly applicable due to its strongly dispersive and lossy nature, and generalized definitions accounting for material dispersion and absorption are required. The values shown here should therefore be interpreted as representative orders of magnitude of optical confinement [8]. For a more consistent comparison of fabrication requirements, we focus on lithographically fabricated nanogap structures, such as bowtie cavities, rather than self-assembled nanocube-based cavities. Nevertheless, the latter may exhibit superior performance in certain optical metrics [4]. The collection efficiencies η_c in (b) are based on waveguide-coupled collection for WGM cavities [23], PhC cavities [5, 32, 33] and slow-light waveguides [35]. In contrast, free-space collection efficiencies are demonstrated for plasmonic [30, 34] and DBR micropillar cavities [25], as directly comparable emitter-to-waveguide collection efficiencies for the relevant cavity modes are not available in the literature considered here. These schemes represent the typical photon-extraction routes for each platform. The relatively low collection efficiency of WGM cavities demonstrated here mainly reflects unoptimized η_{ex}, while high overall collection efficiencies have yet to be directly reported. For clarity, $g^{(2)}(0)$ in (a) and V in (b) are plotted as their reciprocals.

considered metrics. Semiconductor QDs, especially the self-assembled InAs/GaAs QDs, offer a favorable combination of high radiative efficiency, optical transition strength, single-photon purity, and indistinguishability, although their best coherence performance generally requires cryogenic operation. For defects in 2D materials, hexagonal boron nitride (hBN) defects are of particular interest because certain defects exhibit antibunched emission at room temperature while retaining the integration advantages of atomically thin material layers. Nevertheless, hBN hosts a rich variety of defect configurations and emission centers, and the microscopic origins of many emitters have not yet been fully understood. Defects in 2D materials have not yet demonstrated a clear overall advantage over other mature quantum-emitter platforms. The broader appeal of 2D materials lies instead in the rich physics of valley excitonic states in transition metal dichalcogenide materials, such as moiré excitons, together with their electrical and strain tunability. Semiconductor QDs and defect emitters in 2D materials exhibit emitter-to-emitter variations in transition energy, leading to substantial inhomogeneous

wavelength distributions. Color centers in crystals, represented here by NV centers in bulk diamond, can also support room-temperature single-photon generation, although their optical emission contains a substantial phonon sideband. Their zero-phonon line transition frequencies are more reproducible than those of many self-assembled emitters, but remain sensitive to local strain and electric-field fluctuations and may therefore require spectral tuning to bring different centers into resonance. Trapped atomic emitters provide highly reproducible transitions and exceptional coherence because identical atoms share essentially the same discrete energy-level structure. But deterministic atom-photon interfaces typically require stringent conditions such as ultrahigh vacuum, precise trapping, and laser cooling.

The nanophotonic structures provide the other independent degree of freedom for engineering the electromagnetic environment, allowing the optical response of a material platform to be tailored toward specific light–matter interaction requirements. The representative metrics considered here include the quality factor Q, effective mode volume V, experimental Purcell factor F_{P}, structural collection efficiency η_{c}, and critical feature size L. The quality factor Q determines both photon storage time and spectral selectivity, and it is typically extracted from the resonance linewidth in experiments. The effective mode volume V controls the vacuum-field amplitude and therefore the emitter–field coupling strength [8]. The Purcell factor F_{P} provides a direct measure of spontaneous-emission-rate enhancement relative to a reference environment. Experimentally, it is commonly inferred from time-resolved emission measurements by comparing the decay rates of coupled and reference emitters, with nonradiative contributions accounted for when necessary [6]. Here, we used the experimentally reported value for practical comparison, which should be distinguished from the ideal Purcell factor calculated by Eq. (1). Collection efficiency η_{c} characterizes how efficiently photons are directed into and extracted from a useful output channel [12]. The collection efficiency strongly depends on the adopted collection scheme. In particular, waveguide-coupled collection efficiency provides a useful indication of a structure's potential for integration into photonic circuits. However, overall integrability also depends on factors such as fabrication compatibility, device footprint, and scalability. Finally, the critical feature size L provides a practical measure of the characteristic fabrication scale and an indication of the required fabrication resolution, while the overall fabrication complexity also depends on fabrication techniques and the constituent material.

Different nanophotonic structures offer distinct strategies for confining, storing, and routing light. Consequently, they exhibit complementary strengths and limitations across different performance metrics, as illustrated in Fig. 2(b), making them advantageous for different applications. Planar PhC cavities combine wavelength-scale small mode volumes [$\sim(\lambda/n)^3$] with high Q factors up to 10^5 to 10^6 after optimization. Beyond strong optical confinement, their compatibility with planar waveguides also enables efficient routing of cavity-enhanced emission into integrated photonic circuits [5, 32, 33]. However, for free-space emission, PhC defect cavities without careful design do not necessarily provide highly efficient far-field extraction [36], so engineered far-field patterns or circular Bragg grating cavities are often introduced to improve usable photon collection. More importantly, flexible geometric degrees of freedom offered by PhC platforms enable deliberate engineering of dispersion, symmetry, and inter-mode coupling, enabling novel photonic states such as topological and moiré modes [37, 38]. WGM cavities, such as microdisks and microrings, generally exhibit moderate Q factor and V performance, but offer relatively simple designs and fabrication processes [24]. Ideal WGM cavities naturally support degenerate clockwise and counterclockwise propagating modes, making them suitable for chiral photonic devices. Here we focus on relatively small WGM cavities, typically tens of micrometers in size, where reduced mode volumes are advantageous for single-emitter light–matter interactions. Larger resonators with ultrahigh Q are therefore not considered. With similar Q and V performance, DBR micropillars can offer excellent vertical extraction and mode matching to free-space optics or fibers, making free-space collection a commonly adopted output scheme. However, an efficient waveguide extraction scheme for conventional DBR micropillars remains to be demonstrated. In terms of fabrication, WGM and DBR micropillar cavities generally require lower lateral patterning resolution due to their relatively simple geometries. By contrast, plasmonic cavities, such as the bowtie cavities [39], have some of the smallest critical feature sizes among the considered structures, enabling extremely small optical mode volumes by localizing fields in metallic nanogaps. Although their Q factors (about 10^0-10^1) are typically limited by metallic losses, the extreme field confinement still yields some of the largest experimentally reported Purcell enhancements among these structures [30, 34]. The collection efficiency η_{c} of plasmonic cavities is also limited by non-radiative decays, together with finite far-field collection efficiency. Waveguide coupling of plasmonic nanostructures has also been experimentally demonstrated for surface-enhanced Raman scattering [40, 41], indicating the potential of integrating plasmonic cavities with on-chip waveguides. However, these studies do not report directly comparable emitter-to-waveguide efficiencies for cavity-enhanced emission. Therefore, free-space collection efficiencies are adopted in Fig. 2(b). Unlike the cavity-based approaches discussed above, slow-light PhC

waveguides enhance light–matter interactions through dispersion engineering. The reduced group velocity, commonly characterized by the group index, increases the guided optical density of states [37]. This approach can provide a broader enhancement bandwidth than high Q cavities, depending on the dispersion design. In terms of fabrication, slow-light PhC waveguides have critical feature sizes comparable to those of planar PhC cavities, as both rely on similar photonic-crystal patterning. For photon extraction, the enhanced optical mode itself also serves as a transport channel, enabling efficient emitter-waveguide coupling and facilitating photonic integration [35].

Across these different photonic architectures, however, the ideal optical metrics do not fully capture the experimentally achievable light–matter interaction, as the overall performance is also constrained by emitter–cavity matching, fabrication imperfections, and material-related effects. Experimental Purcell factors are considered separately from the ideal Q and V metrics, as the measured enhancement is often lower than the value predicted by Eq. (1) [Fig. 2(b)], which assumes perfect spatial, polarization, and spectral matching between a narrowband emitter and a single cavity mode. In real devices, displacement from the field maximum, dipole misalignment, spectral detuning, emitter linewidth and spectral diffusion can all reduce the effective interaction [6]. Fabrication imperfections further modify the designed optical mode, as surface roughness and geometric disorder can lower the practical Q [24]. Importantly, reducing the mode volume also introduces additional constraints that are not captured by the ideal Q/V metric. In dielectric nanocavities, extreme confinement often places the emitter closer to etched interfaces, air holes, or surfaces, where charge traps, strain, and local electric-field fluctuations can degrade the emitter linewidth, spectral stability, and quantum efficiency [24]. This trade-off is especially relevant for semiconductor QDs, which possess a finite spatial extent and therefore cannot always be treated as point-like dipoles in highly nonuniform optical fields. As the optical mode is compressed to dimensions comparable to the emitter size or to the spatial scale of material inhomogeneity, the local-field distribution across the emitter and interface-induced perturbations may become non-negligible. Besides, for metallic structures, the enhanced electromagnetic LDOS near the metal surface competes with nonradiative energy transfer and Ohmic dissipation, which can ultimately lead to fluorescence quenching [4, 13]. At nanometer and subnanometer gap scales, the local-response description of classical electrodynamics can become insufficient. Nonlocal electronic screening and electron spill-out modify the induced charge distribution and local fields, while at sufficiently small separations, electron tunneling can qualitatively reshape the plasmonic modes [42]. Thus, maximizing the nominal Q/V ratio does not necessarily maximize the useful radiative output or the overall quality of the light–matter interface.

Engineering light–matter interactions through material selection and nanophotonic design enables a broad range of applications. Distinct coupling regimes lead to different physical behaviors and applications. Figure 3 illustrates representative applications associated with weak and strong coupling. In the weak-coupling regime, quantum light sources represent one of the most important applications. Purcell-enhanced radiative decay leads to an increased emission rate and thereby increased brightness [4]. Meanwhile, preferential enhancement of the desired emission channel relative to background or competing transitions can improve the measured single-photon purity and thereby reduce $g^{(2)}(0)$ for practical and high-performance single photon sources [4, 5, 35]. When radiative emission is accelerated relative to dephasing, this acceleration also improves photon indistinguishability [5], which is particularly important in applications like photonic quantum information processing [8]. With strong spatial overlap between the optical mode and the gain medium, nanolasers can also benefit from the Purcell effect, which enhances spontaneous emission into the desired cavity mode and increases the spontaneous-emission coupling factor, thereby reducing the lasing threshold [43]. The enhanced local field can also amplify the inherently weak optical responses of materials, leading to applications in high-sensitivity detection techniques such as surface-enhanced Raman scattering or surface-enhanced infrared absorption spectroscopy [42]. Entering the strong-coupling regime, the hybrid light–matter states provide a natural building block for cavity-mediated quantum gates and photon–matter quantum interfaces. Such interfaces can support coherent state transfer, photon-mediated interactions, and entanglement generation between stationary and flying qubits [6, 7]. In systems containing a large ensemble or a collective excitonic excitation, strong coupling gives rise to hybrid exciton–photon polaritons, which combine the low effective mass of their photonic component with matter-mediated interactions [44]. This combination enables collective phenomena such as polariton condensation and nonequilibrium Bose–Einstein-condensation-like behavior [45]. Extending strong coupling to multiple emitters or coupled photonic modes further enables analog quantum simulation, in which engineered photon-mediated interactions reproduce effective many-body Hamiltonians and collective quantum dynamics that are difficult to access in natural systems [46].

Looking beyond the nanophotonic structures discussed here, quasi-bound states in the continuum [47], metasurfaces [48], moiré PhC cavities [38] and hybrid dielectric-plasmonic architectures [39] also provide routes to control light–matter interaction. Chiral and topological photonic designs further extend this control to properties

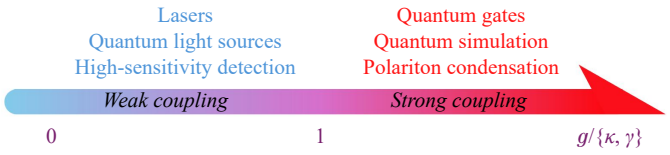


Fig. 3 Representative applications associated with weak and strong light–matter coupling. The weak-coupling regime supports applications such as quantum light sources, nanolasers, and high-sensitivity detection, whereas the strong-coupling regime enables exciton-polariton condensation and provides useful resources for photon-emitter quantum gates and quantum simulation. This classification highlights typical applications associated with each coupling regime, although some applications can also be realized in the other regime through specially designed schemes.

such as directionality, polarization, and robustness, rather than simply increasing the scalar interaction strength [37, 49]. The rapidly developing fields of time-varying photonics and Floquet systems may further enrich these platforms by introducing a temporal degree of freedom, enabling reconfigurable devices and functionalities inaccessible to static structures such as parametric amplification without phase matching or magnetless nonreciprocity [50, 51]. As the available degrees of freedom continue to expand, the key question is no longer how to maximize a single optical figure of merit, but how to translate these capabilities into a functional and experimentally robust light–matter interface. This requires simultaneous control over emitter position, transition frequency, dipole orientation, optical confinement, and photon extraction. Co-design of the quantum emitter, electromagnetic mode, and output channel is therefore likely to be essential for converting record local enhancement into reproducible and scalable quantum and optoelectronic devices.

Declarations The authors declare that they have no competing interests and there are no conflicts.

Acknowledgements This work was supported by the National Key Research and Development Program of China (Grant No. 2021YFA1400700) and the National Natural Science Foundation of China (Grant Nos. 12494600, 12494603, 22461142143, 12521004, and 12404354).

References

1. Z. K. Ma, S. Y. Wu, H. C. Li, X. Q. Chen, K. Peng, C. J. Qian, K. J. Jin, Q. H. Gong, and X. L. Xu, Recent progress and applications of III–V quantum dots in quantum technologies, *Appl. Phys. Rev.* 13(1), 011313 (2026)
2. L. Novotny and B. Hecht, Principles of Nano-Optics, 3rd Ed., Cambridge: Cambridge University Press, 2025
3. E. M. Purcell, Spontaneous emission probabilities at radio frequencies, *Phys. Rev.* 69, 681 (1946)
4. T. B. Hoang, G. M. Akselrod, and M. H. Mikkelsen, Ultrafast room-temperature single photon emission from quantum dots coupled to plasmonic nanocavities, *Nano Lett.* 16(1), 270 (2016)
5. F. Liu, A. J. Brash, J. O'Hara, L. M. P. P. Martins, C. L. Phillips, et al., High Purcell factor generation of indistinguishable on-chip single photons, *Nat. Nanotechnol.* 13(9), 835 (2018)
6. P. Lodahl, S. Mahmoodian, and S. Stobbe, Interfacing single photons and single quantum dots with photonic nanostructures, *Rev. Mod. Phys.* 87(2), 347 (2015)
7. C. J. Qian, X. Xie, J. N. Yang, K. Peng, S. Y. Wu, et al., Enhanced strong interaction between nanocavities and *p*-shell excitons beyond the dipole approximation, *Phys. Rev. Lett.* 122(8), 087401 (2019)
8. A. González-Tudela, A. Reiserer, J. J. García-Ripoll, and F. J. García-Vidal, Light–matter interactions in quantum nanophotonic devices, *Nat. Rev. Phys.* 6(3), 166 (2024)
9. P. G. Eliseev, H. Li, A. Stintz, G. T. Liu, T. C. Newell, K. J. Malloy, and L. F. Lester, Transition dipole moment of InAs/InGaAs quantum dots from experiments on ultralow-threshold laser diodes, *Appl. Phys. Lett.* 77(2), 262 (2000)
10. D. Riedel, I. Söllner, B. J. Shields, S. Starosielec, P. Appel, E. Neu, P. Maletinsky, and R. J. Warburton, Deterministic enhancement of coherent photon generation from a nitrogen-vacancy center in ultrapure diamond, *Phys. Rev. X* 7(3), 031040 (2017)
11. S. Doan, S. D. Patel, Y. L. Chen, J. A. Gusdorff, M. E. Turiansky, et al., High-performance near-infrared quantum emission from color centers in hBN, *ACS Nano* 20(27), 19209 (2026)
12. M. Esmann, S. C. Wein, and C. Antón-Solanas, Solid-state single-photon sources: Recent advances for novel quantum materials, *Adv. Funct. Mater.* 34(30), 2315936 (2024)
13. I. P. Radko, M. Boll, N. M. Israelsen, N. Raatz, J. Meijer, F. Jelezko, U. L. Andersen, and A. Huck, Determining the internal quantum efficiency of shallow-implanted nitrogen–vacancy defects in bulk diamond, *Opt. Express* 24(24), 27715 (2016)
14. D. B. Higginbottom, L. Slodička, G. Araneda, L. Lachman, R. Filip, M. Hennrich, and R. Blatt, Pure single photons from a trapped atom source, *New J. Phys.* 18(9), 093038 (2016)
15. D. A. Steck, Rubidium 87 D Line Data, University of Oregon, 2025
16. C. Fournier, A. Plaud, S. Roux, A. Pierret, M. Rosticher, et al., Position-controlled quantum emitters with reproducible emission wavelength in hexagonal boron nitride, *Nat. Commun.* 12(1), 3779 (2021)
17. J. F. Zhang, S. Chattaraj, Q. Huang, L. Jordao, S. Y. Lu, and A. Madhukar, On-chip scalable highly pure and indistinguishable single-photon sources in ordered arrays: path to quantum optical circuits, *Sci. Adv.* 8(35), eabn9252 (2022)
18. C. Kurtsiefer, S. Mayer, P. Zarda, and H. Weinfurter, Stable solid-state source of single photons, *Phys. Rev. Lett.* 85(2), 290 (2000)

19. E. Schöll, L. Hanschke, L. Schweickert, K. D. Zeuner, M. Reindl, et al., Resonance fluorescence of GaAs quantum dots with near-unity photon indistinguishability, *Nano Lett.* 19(4), 2404 (2019)
20. C. Fournier, S. Roux, K. Watanabe, T. Taniguchi, S. Buil, J. Barjon, J. P. Hermier, and A. Delteil, Two-photon interference from a quantum emitter in hexagonal boron nitride, *Phys. Rev. Appl.* 19(4), L041003 (2023)
21. H. Bernien, L. Childress, L. Robledo, M. Markham, D. Twitchen, and R. Hanson, Two-photon quantum interference from separate nitrogen vacancy centers in diamond, *Phys. Rev. Lett.* 108(4), 043604 (2012)
22. F. Dubin, D. Rotter, M. Mukherjee, S. Gerber, and R. Blatt, Single-ion two-photon source, *Phys. Rev. Lett.* 99(18), 183001 (2007)
23. S. Ates, I. Agha, A. Gulinatti, I. Rech, A. Badolato, and K. Srinivasan, Improving the performance of bright quantum dot single photon sources using temporal filtering via amplitude modulation, *Sci. Rep.* 3(1), 1397 (2013)
24. N. Kryzhanovskaya, A. Zhukov, E. Moiseev, and M. Maximov, III–V microdisk/microring resonators and injection microlasers, *J. Phys. D: Appl. Phys.* 54(45), 453001 (2021)
25. H. Wang, J. Qin, S. Chen, M. C. Chen, X. You, et al., Observation of intensity squeezing in resonance fluorescence from a solid-state device, *Phys. Rev. Lett.* 125(15), 153601 (2020)
26. C. Arnold, V. Loo, A. Lemaître, I. Sagnes, O. Krebs, P. Voisin, P. Senellart, and L. Lanco, Optical bistability in a quantum dots/micropillar device with a quality factor exceeding 200 000, *Appl. Phys. Lett.* 100(11), 111111 (2012)
27. K. Srinivasan, M. Borselli, O. Painter, A. Stintz, and S. Krishna, Cavity Q, mode volume, and lasing threshold in small diameter AlGaAs microdisks with embedded quantum dots, *Opt. Express* 14(3), 1094 (2006)
28. W. Fang, J. Y. Xu, A. Yamilov, H. Cao, Y. Ma, S. T. Ho, and G. S. Solomon, Large enhancement of spontaneous emission rates of InAs quantum dots in GaAs microdisks, *Opt. Lett.* 27(11), 948 (2002)
29. A. Faraon, C. Santori, Z. H. Huang, V. M. Acosta, and R. G. Beausoleil, Coupling of nitrogen–vacancy centers to photonic crystal cavities in monocrystalline diamond, *Phys. Rev. Lett.* 109(3), 033604 (2012)
30. Y. Luo, E. D. Ahmadi, K. Shayan, Y. C. Ma, K. S. Mistry, C. J. Zhang, J. Hone, J. L. Blackburn, and S. Strauf, Purcell-enhanced quantum yield from carbon nanotube excitons coupled to plasmonic nanocavities, *Nat. Commun.* 8(1), 1413 (2017)
31. H. Siampour, C. O'Rourke, A. J. Brash, M. N. Makhonin, R. Dost, D. J. Hallett, E. Clarke, P. K. Patil, M. S. Skolnick, and A. M. Fox, Observation of large spontaneous emission rate enhancement of quantum dots in a broken-symmetry slow-light waveguide, *npj Quantum Inf.* 9, 15(1) (2023)
32. A. Enderlin, Y. Ota, R. Ohta, N. Kumagai, S. Ishida, S. Iwamoto, and Y. Arakawa, High guided mode–cavity mode coupling for an efficient extraction of spontaneous emission of a single quantum dot embedded in a photonic crystal nanobeam cavity, *Phys. Rev. B* 86(7), 075314 (2012)
33. A. Fujita, N. Pholsen, S. Ji, T. Kamei, M. Okano, M. Kakuda, S. Iwamoto, Y. Arakawa, and Y. Ota, Quantum-dot single-photon source based on a two-dimensional photonic crystal nanocavity transfer-printed on a Si wire waveguide, *J. Appl. Phys.* 138(10), 104401 (2025)
34. J. H. Song, J. Kim, H. Jang, I. Yong Kim, I. Karnadi, J. Shin, J. H. Shin, and Y. H. Lee, Fast and bright spontaneous emission of Er^{3+} ions in metallic nanocavity, *Nat. Commun.* 6(1), 7080 (2015)
35. R. Uppu, F. T. Pedersen, Y. Wang, C. T. Olesen, C. Papon, et al., Scalable integrated single-photon source, *Sci. Adv.* 6(50), eabc8268 (2020)
36. K. H. Madsen, S. Ates, J. Liu, A. Javadi, S. M. Albrecht, I. Yeo, S. Stobbe, and P. Lodahl, Efficient out-coupling of high-purity single photons from a coherent quantum dot in a photonic-crystal cavity, *Phys. Rev. B* 90(15), 155303 (2014)
37. H. C. Li, S. Yan, Z. K. Ma, R. Zhu, H. Q. Liu, et al., Chiral quantum optics with topological photonic crystal waveguide of triangular lattice, *Laser Photonics Rev.* 20(11), e01893 (2026)
38. S. Yan, H. C. Li, J. N. Yang, X. Q. Chen, H. Q. Liu, et al., Cavity quantum electrodynamics with moiré photonic crystal nanocavity, *Nat. Commun.* 16(1), 4634 (2025)
39. B. W. Fu, W. S. Dai, L. L. Yang, D. J. Dai, J. N. Yang, et al., Enhanced light–matter interaction with Bloch surface wave modulated plasmonic nanocavities, *Nano Lett.* 25(2), 722 (2025)
40. F. Peyskens, P. Wuytens, A. Raza, P. Van Dorpe, and R. Baets, Waveguide excitation and collection of surface-enhanced Raman scattering from a single plasmonic antenna, *Nanophotonics* 7(7), 1299 (2018)
41. J. Redolat, D. Arenas-Ortega, Á. Barreda, A. Griol, E. Pinilla-Cienfuegos, and A. Martínez, Polarization-insensitive integration of nanoparticle-on-a-slit cavities with dielectric waveguides for on-chip surface enhanced Raman spectroscopy, *npj Nanophoton.* 2(1), 17 (2025)
42. D. D. Song, Z. Y. Lu, Q. B. Guo, T. Z. Zhang, J. M. Ji, et al., Enhanced light–matter interaction in plasmonic nanocavities: Principle, challenge, and perspective, *Photonics Insights* 5(1), R01 (2026)
43. W. X. Zhang, X. Xie, H. M. Hao, J. C. Dang, S. Xiao, et al., Low-threshold topological nanolasers based on the second-order corner state, *Light: Sci. Appl.* 9(1), 109 (2020)
44. D. S. Dovzhenko, S. V. Ryabchuk, Y. P. Rakovich, and I. R. Nabiev, Light–matter interaction in the strong coupling regime: Configurations, conditions, and applications, *Nanoscale* 10(8), 3589 (2018)
45. K. Peng, W. Li, M. Sun, J. D. H. Rivero, C. Ti, X. Han, L. Ge, L. Yang, X. Zhang, and W. Bao, Topological valley hall polariton condensation, *Nat. Nanotechnol.* 19(9), 1283 (2024)
46. K. Peng, W. Li, N. G. Berloff, X. Zhang, and W. Bao, Room temperature polaritonic soft-spin XY Hamiltonian in organic–inorganic halide perovskites, *Nanophotonics* 13, 2651 (2024)
47. G. Wan, Y. Xue, X. Huang, J. X. Zeng, Z. W. Zheng,

Y. Chen, and X. X. Zhou, Broadband and highly efficient enhancement of photonic spin hall effect at a quasi-bound state in the continuum, *Front. Phys. (Beijing)* 20(5), 052203 (2025)

48. Y. Yuan, C. J. Qian, L. L. Yang, X. C. Ru, Y. L. Li, et al., Robust Purcell effect of $CsPbI_3$ quantum dots using nonlocal plasmonic metasurfaces, *Phys. Rev. Lett.* 134(24), 243804 (2025)
49. Y. Liu and J. H. Jiang, Photonic biosensing through cascade-coupled Su–Schrieffer–Heeger boundary modes, *Front. Phys. (Beijing)* 20(4), 044203 (2025)
50. M. M. Asgari, P. Garg, X. C. Wang, M. S. Mirmoosa, C. Rockstuhl, and V. Asadchy, Theory and applications of photonic time crystals: a tutorial, *Adv. Opt. Photon.* 16(4), 958 (2024)
51. A. C. Valero, S. Gladyshev, D. Globosits, S. Rotter, E. A. Muljarov, and T. Weiss, Revealing the resonant physics of open photonic time crystals, *Laser Photonics Rev.* e71318 (2026)